

Contents lists available at ScienceDirect

# Colloids and Surfaces A: Physicochemical and Engineering

journal homepage: http://ees.elsevier.com



# Stability of nanobubbles in different salts solutions

Shaini Aluthgun Hewage, Jitendra Kewalramani, Jay N. Meegoda \*

Department of Civil & Environmental Engineering, New Jersey Institute of Technology, Newark, NJ, 07102, United States

#### ARTICLE INFO

#### Keywords Stability Nanobubbles Salts solutions Zeta potential Diffused double layer

#### ABSTRACT

The stability of nanobubbles in electrolyte solutions under different ion valence values was studied using deionized water, NaCl, Na<sub>2</sub>SO<sub>4</sub>, Na<sub>3</sub>PO<sub>4</sub>, CaCl<sub>2</sub> and FeCl<sub>3</sub>. Nanobubbles were generated using hydrodynamic cavitation, and bubbles were tested for size and zeta potential. All the samples were stable for one week with no significant deviation in either bubble size or zeta potential values. The variation of size and zeta potential among six samples can be attributed to the solution properties and was mainly dependent on solution pH and the cation valency. The ion profiles revealed that the cation concentration at the bubble surface was higher than that of bulk, confirming that the bubbles were negatively charged for neutral and high pH values (≥ 4) under low valency cation adsorption. The high valency cations have the potential to neutralize or completely reverse the bubble charge. Anions or co-ions have minimal effect on the surface potential or the surface charge. The calculated internal pressures of bubble were unrealistically high, suggesting that the surface tension should be lower than that of water for nanobubble solutions. The interaction energy profile shows no significant energy barrier that overcomes the attractive van der Waals forces for all the solutions, except NaCl which had a  $1.87 \times 10^{-20} \, \mathrm{J}$  barrier at a 5 nm separation distance. However, with the recorded stable bubbles, the calculation of the attractive van der Waals forces produced unrealistic values indicating that the Hamaker constant used for the calculation may not be valid at the nanobubble gas-liquid interface. This revealed that nanobubbles should contain exceptional interfacial properties that need to be carefully investigated and evaluated.

# 1. Introduction

Bulk nanobubbles are gas-filled cavities suspended in aqueous solutions having diameters smaller than 200 nm [1–3]. The existence of these extremely small bubbles has been experimentally confirmed by different researchers [3,4]. These bubbles have attracted attention due to their extraordinary properties and characteristics, especially their long lifespans and electrically charged interfaces [5,6]. Nanobubbles are already used in a wide range of applications and areas, including drinking/wastewater/groundwater treatment [7–10], decontamination of sediments and soils [11–14], biomedical engineering [15–17], and the agricultural, fishing, and food industries [2,18–20]. Despite their widespread use, nanobubbles remain a poorly understood technology, especially relating to their long existence or stability, interfacial properties, and radical formation.

The stability and reactivity of nanobubbles depend on several factors, such as the bubble size, zeta potential, and interfacial characteristics [21–25]. Nanobubble characteristics also highly depend on solution properties, infilled gas type, and the energy provided to the system to generate nanobubbles [18]. Solution properties such as temperature, pressure, ion type, ion concentration, pH, presence of organic matters

or impurities, presence of surfactants, and saturated gas concentration play an important role [23,26–28]. The infilled gas type and its solubility and reactivity can also impact the bubble properties [18,27,29]. Furthermore, the generation mechanism and energy provided to the system (i.e., hydrodynamic method, ultrasound) are key factors that influence the bubble size, radical formation, and related chemical reactions [30–32].

Nanobubbles have an electrical charge interface which controls the ion distribution in aqueous solution near the bubble surface. The accumulation of ions near the gas-liquid interface influences the physical-chemical properties of the nanobubble. An application such as the flotation can be benefited by controlling the number of charges on nanobubbles. Hence, with the proper selection of electrolyte types and concentrations, the zeta potential of bubbles and the bubble stability can be controlled. The bubbles formed in the different electrolyte solutions can be used to further understand the nanobubble properties. Even though there are prior studies on nanobubbles formed in different electrolyte solutions, research findings and conclusions are only limited to the direct comparison of zeta potential values and specific adsorption with respect to the valency effect. Limited research has conducted on the application of DLVO theory for nanobubbles formed in multiva-

<sup>\*</sup> Corresponding author.

E-mail address: meegoda@njit.edu (J.N. Meegoda)

lent electrolytes, as most of the prior research is limited to nanobubbles formed in symmetrical electrolytes. The present study provides experimental data on bubble sizes and zeta potential values for nanobubbles formed in different electrolyte solutions at both the generation and after one week to evaluate the long-term stability. The diffuse double layer theory was applied to calculate the potential distribution and ion distribution away from the bubble surface, and the DLVO theory applied for different electrolyte solutions by considering both the interactions of electrostatic repulsion and van der Waals attraction. The analyzed results were collectively considered to evaluate the properties and behavior of nanobubbles. Additionally, a literature review was conducted for nanobubbles in different valency electrolytes to provide a meaningful comparison with respect to the work presented in this manuscript.

In this research, nanobubbles were generated in different electrolyte solutions under different ion valences and ionic strengths, namely deionized water and NaCl,  $\rm Na_2SO_4$ ,  $\rm Na_3PO_4$ ,  $\rm CaCl_2$ , and  $\rm FeCl_3$  in deionized water. The diffuse double layer theory was applied to nanobubbles in the monovalent electrolyte of NaCl for different concentrations and found stable nanobubbles were formed in low concentration (0.001 M) solution [33]. Therefore, in this research, a concentration of 0.001 M for the various electrolytes was used to generated nanobubbles to study the impact of different ion types on characteristics and behavior of nanobubbles.

# 2. Formation of electric double-layer around nanobubbles

Nanobubbles suspended in aqueous solutions carry electrical charges on the gas-liquid interface [18,26,33]. The nanobubble with an electrical charge interface accumulates counter charges in order to preserve electrical neutrality. For example, negatively charged surfaces are attracted to positively charged cations for electrostatic equilibrium. Simultaneously, due to ion diffusion, the cations move to the bulk solution, and the diffused layer is formed. At the diffused layer, the concentration of counterions is increased towards the bubble surface, and ion distribution primarily depends on the magnitude of the surface charge. In contrast, like charges (co-ions) are repelled away from the bubble surface, and there is a low concentration of co-ions at the interface. This diffuse ion distribution has been formulated by different models to evaluate the surface charge density and distribution of ions around the colloidal particles.

The Poisson-Boltzmann (PB) equation can be used to describe the distribution of ions around the charged particle and can calculate the electric potential,  $\psi(x)$ , around the surface. The non-linear second order PB equation can be solved subjected to the boundary conditions and then can be related to the surface charged density. No analytical solutions are available for the PB equation for the general case of spherical particles. However, there are a number of methods used to determine numerical solutions. In this analysis, due to the spherical colloidal condition along with asymmetric ionic valency conditions, the general nonlinear PB equation must be solved. Therefore, in this manuscript, we utilized the numerical simulation based on the network simulation method [34].

The network simulation method consists of modeling the governing equations by means of an electrical circuit. This network simulation method is useful as it avoids difficulties of mathematical analysis. The model consists of a graphical analogous representation of the physical process of the diffuse double layer to electrical circuit diagrams which are analyzed using an electric circuit simulation program. In this work, PSpice electric circuit simulation program was used for the analysis. The full details of the network model used in this manuscript can be found in [34].

## 3. The bubbles interaction force and energy

The classical DLVO theory can be used to explain the interaction between nanobubbles suspended in an electrolyte solution. The stability of the bubble can be considered based on the energy or force balance between the attractive van der Waals interaction and the repulsive electric double layer interactions [35,36]. The relevant equations are given in the next section.

#### 4. Equations for modeling

Consider the spherical nanobubble with radius a, stern layer thickness d, and zeta potential,  $\zeta$ . In this research, the zeta potential is assumed as equal to the Stern potential ( $\zeta \cong \Psi d$ ) and the justification for this assumption can be found in [33]. The Poisson–Boltzmann equation for a spherical charged particle immersed in an infinite electrolyte solution relates the electric potential  $\Psi(r)$  to the charge density  $\rho(r)$  at any point of the diffuse electric double layer given by [34],

$$\frac{1}{r^2} \frac{d}{dr} \left[ r^2 \frac{d\psi(r)}{dr} \right] = -\frac{\rho(r)}{\varepsilon}$$

$$= -\frac{1}{\varepsilon} \sum_{i=1}^{N} z_i e n_i^0 exp\left(\frac{-z_i e \psi(r)}{kT}\right) \tag{1}$$

Here, we consider the boundary condition  $\psi$  (r = a + d) =  $\psi$ <sub>stern</sub> =  $\zeta$  and  $\psi$  ( $r \to \infty$ ) = 0, where,  $\varepsilon$  is the dielectric permittivity of the solution,  $z_i$  and  $n_i^0$  are valency and bulk concentrations ( $ions/m^3$ ) of the i th ionic species respectively,  $\varepsilon$  is an elementary charge (1.60217662 × 10<sup>-19</sup> C),  $\varepsilon$  is Boltzmann constant (1.380649 × 10<sup>-23</sup> J·K<sup>-1</sup>), and T is temperature ( $\varepsilon$ ).

In order to simplify Eq. (1), the dimensionless variables are needed as shown below,

$$y = \frac{e\psi(r)}{kT} q = Kr \tag{2}$$

where the Debye length  $(K^{-1})$  or diffuse double layer characteristic length can be expressed as,

$$K^{-1} = \sqrt{\frac{\varepsilon kT}{e^2 \sum_{i=1}^{N} z_i^2 n_i^0}}$$
 (3)

Now Eq. (1) can be updated,

$$\frac{1}{q^2} \frac{d}{dq} \left[ q^2 l \right] = \overline{\rho} \left( y \right) \tag{4}$$

with

$$\bar{\rho}(y) = \frac{\sum_{i=1}^{N} z_i n_i^0 \exp\left(-z_i y\right)}{\sum_{i=1}^{N} z_i^2 n_i^0}$$
 (5)

and

$$l = -\frac{dy}{dq} \tag{6}$$

The boundary condition for Eq. (1) becomes,

$$y(q = q_{stern}) = y_{stern} \quad y(q \to \infty) = 0$$
 (7)

with

$$y_d = \frac{e\psi_{stern}}{kT} = \frac{e\zeta}{kT} q_{stern} = K(a+d)$$
 (8)

The surface charge density (  $\sigma_0$ ) and potential ( $\Psi$ ) relationship can be expressed as,

$$\sigma_0 = -\epsilon \left(\frac{d\psi(r)}{dr}\right)_{r=(a+d)} \tag{9}$$

Therefore, the surface potential  $(\psi_0)$  can be calculated as,

$$\psi_0 = \psi_{stern}^{drop} + \zeta \tag{10}$$

The stern layer can be considered as a parallel concentric sphere capacitor, and therefore the potential drop is linear within the stern layer. Hence  $\psi_{stern}^{drop}$  is,

$$\psi_{stern}^{drop} = \sigma_0 \left( \frac{d}{\epsilon} \right) \tag{11}$$

Once the potential distribution is solved, the ionic concentration at any point  $(n_i(r))$  of the double layer is given by the Boltzmann distribution of ions i at distance r,

$$\mathbf{n}_{i}(r) = n_{i}^{0} exp\left(\frac{z_{i}e\psi(r)}{kT}\right) \tag{12}$$

The ionic strength of the electrolyte solution is a measure of the concentration of ions in that solution, and given by,

$$I = \frac{1}{2} \sum_{i} n_i^0 z_i^2 \quad (m^{-1}) \tag{13}$$

Once the surface charge densities and surface potential calculations were obtained, the interaction between the particles can be found based on the DLVO theory by considering electrostatic repulsion and Van der Waals attraction.

For low surface potential, below about 25 mV, for two spheres of radius, R with identical charges, the electrostatic interaction force F(D) and energy W(D) for separation distance D are given by [37],

$$F(D) \approx 2\pi R \varepsilon K \psi_0^2 e^{-KD} = 2\pi R \sigma^2 e^{-KD} / K \varepsilon \quad (N)$$
 (14)

$$W(D) \approx 2\pi R \varepsilon \psi_0^2 e^{-KD} = 2\pi R \sigma^2 e^{-KD} / K^2 \varepsilon \quad (J)$$
 (15)

The above equations (Eqs. 14 and 15) are valid for all the electrolytes (i.e., 1:1, 1:2, 2:2, 3:1, or mixtures) with appropriate Debye lengths.

The attractive van der Waals interaction for two spherical surfaces with radius, R for all the separation distances (D < R) can be expressed as [35].

$$F(D) = -\frac{AR}{12D^2} \quad (N)$$
 (16)

$$W(D) = -\frac{AR}{12D} \quad (J) \tag{17}$$

where A is the Hamaker's constant.

The van der Waals forces are effective at a short-range around a distance of 10 nm. When the two bubbles approach, a thin-film is formed between them. As a result, excess surface salt in the thin film is higher than that on the bubble surface. It can reverse the direction of force at the bubble, which can weaken the van der Waals attraction force. Further, with significant salt concentration, the surface tension of the liquid film will increase, and concurrently will reduce the surface tension of the bulk fluid close to approaching bubbles. Likewise, the nanobubbles are believed to be stabilized by adsorbed impurities and ions at the gas-liquid interface. Therefore to represent this weakened van der Waals forces, the Hamaker constant of  $2\times 10^{-20}\,J$  was used [38] for the nanobubbles in electrolyte solutions, instead of the bubble-bubble interaction across pure water which has a Hamaker constant of

 $3.7 \times 10^{-20} J$  [35]. However, the Hamaker constants used in van der Waals attractive force calculations in this manuscript do not explicitly depend on specific properties of salt ions [39].

One of the main features of nanobubbles are their estimated high internal pressure values. These high internal pressures and the long-term stability of nanobubbles are very debatable facts. One of the suggested rational for the stability of the nanobubble is associated with the surface charge at the gas/liquid interface which introduces opposing forces to the surface tension that prevents the gas dissipation. Therefore, with the assumption that the nanobubble attains mechanical equilibrium, the nanobubbles pressure difference can be expressed using the Modified Young Laplace Equation [33],

$$[P_{in} - P_{out}] = \frac{2\gamma}{R} - \frac{2\pi\sigma^2}{\epsilon}$$
 (18)

# 5. Experimental procedure

### 5.1. Materials

Sodium Chloride (NaCl, 99+%), and Sodium Sulfate (Na<sub>2</sub>SO<sub>4</sub>, 99+%), from ACROS Organics and Sodium Phosphate Tribasic Dodecahydrate (Na<sub>3</sub>PO<sub>4</sub>·12H<sub>2</sub>O, 98–102%), Calcium Chloride Dihydrate (CaCl<sub>2</sub>·2H<sub>2</sub>O, 99.0–105.0%), Ferric Chloride Hexahydrate (FeCl<sub>3</sub>·6H<sub>2</sub>O, 97–102%), from Fisher Chemical, and Calcium Chloride Dihydrate (CaCl<sub>2</sub>·2H<sub>2</sub>O, 99+%), from Mallinckrodt, Inc were purchased. For all the experiments, de-ionized water (Millipore DIRECT-Q 3 UV system, Millipore Corporation) was used. The de-ionized water had an electrical conductance of 0.04  $\mu$  S/cm, and fresh DI water was collected in a 100 L tank and allowed to reach equilibrium with the atmospheric gases at room temperature for 24 h.

# 5.2. Preparation of nanobubble

To form nanobubbles in the electrolyte solution, the required amount of salt was measured and dissolved in 250 mL of DI water. Water was added to reach a total volume of 18 L and the solution was placed in a 25 L chamber (e.g., for NaCl (99+%), 1.052 g of NaCl dissolved in 18 L of DI water to obtain 0.001 M solution [(1/(58.44 g/ mol))  $\times$  1.052 g  $\times$  (1/18 L)]. The nanobubbles were formed using the micro-nano nozzle (model BT-50FR, Riverforest Corporation, USA), which utilizes the hydrodynamic cavitation method. The solution was allowed to pass through the nano nozzle using a 55 psi water pump (model 4CUK6, Dayton, USA), where the pump ran for three minutes. All experiments were carefully performed to avoid possible contamination. Two separate experiments were performed for each salt type, and for each test, two samples were tested for bubble size, zeta potential and conductivity with each analyze having six readings (total of 24 records per solution). The solution conductivity was measured to confirm the accuracy of the salt concentration.

# 5.3. Measurement of zeta-potential and nanobubble size

Immediately after the generation and one week after, the nanobubbles were tested for bubble size and  $\zeta$  potential value using the Malvern Zetasizer Nano ZS. The Zetasizer utilizes dynamic light scattering with Non-Invasive Backscatter (NIBS) optics for the size measurements and electrophoretic light scattering technique for the zeta potential measurements. Here, zeta potential was measured by determining the electrophoretic mobility of the particles and then applying Henry's equation based on the Smoluchowisk's approximation. All the tests were performed at room temperature, and the collected samples were stored in airtight flasks for one week for measurements.

# 6. Results and discussion

Table 1 shows solution parameters for the six samples used. It represents the solution type (Col. A), solution concentration (Col. B), molar mass of salt (Col. C), the charge density of cation (Col. D), ionic strength of the salt (Col. E), Debye length (Col. F), the average conductivity at week 0 and week 1 (Col. G,H), average pH at week 0 (Col. I) and average DO concentration at week 0 (Col. J). The dissolved oxygen (DO) concentrations are relatively high compared to ordinary conditions (above 6.5–8 mg/L). For all the samples, the DO concentration was relatively similar and were around 33  $\pm$  0.89 mg/L. Therefore, solution gas concentrations were considered to have reached supersaturation.

Fig. 1a and b show the nanobubbles size variation for six aqueous solutions just after generation and after 1 week, respectively. At gener-

ation, the bubble size increase in order of  $FeCl_3 < Na_3PO_4 < Na_2SO_4 < NaCl < DI$  water  $< CaCl_2$  solutions. The percentage of bubble size growth over 1 week is shown in Fig. 1b, and  $Na_3PO_4$  shows the smallest change (  $\sim 8\%$ ), and  $Na_2SO_4$  (  $\sim 400$  %) shows significant growth. However, all the solutions had stable bubbles with recorded diameters well below 1µm. The percentage of bubble growth increases in the order of  $Na_3PO_4 < NaCl = DI$  water  $< FeCl_3 < CaCl_2 < Na_2SO_4$  solutions.

Fig. 1c and d show the zeta potential just after generation and after 1 week, respectively. All the solutions had negative zeta potential values except for FeCl<sub>3</sub>, which had positive zeta potentials of 10.93 mV initially and 5.07 mV after 1 week. The magnitude of negative zeta potential increased for the other five samples as CaCl<sub>2</sub> < Na<sub>2</sub>SO<sub>4</sub>  $\approx$  NaCl  $\approx$  DI < Na<sub>3</sub>PO<sub>4</sub>. In addition, Fig. 1c shows the pH variation for all six

**Table 1**The solution properties and parameters.

(A)	(B)	(C)	(D)	(E)	(F)	(G)	(H)	(I)	(J)	
Solution	Concentration	Molar Mass	The charge density of cation	Ionic Strength	Ionic Strength Debye length		Average Conductivity		I DO2 concentration	
						Week 0	Week 1	Week 0	Week 0	
	(M)	(g/mol)	(C/mm <sup>3</sup> )	(mol/m <sup>3</sup> )	(nm)	(mS/cm)	(mS/cm)	(-)	(mg/l)	
H <sub>2</sub> O	10 <sup>-7</sup>					0.023	0.024	6.27	31.99	
NaCl	$10^{-3}$	58.44	24	1.00	9.63	0.129	0.131	6.38	32.77	
Na <sub>2</sub> SO <sub>4</sub>	$10^{-3}$	142.04	24	3.00	4.54	0.267	0.276	7.17	33.82	
Na <sub>3</sub> PO <sub>4</sub>	$10^{-3}$	163.94	24	6.00	2.57	0.415	0.351	10.75	34.20	
CaCl <sub>2</sub>	$10^{-3}$	110.98	52	3.00	4.54	0.253	0.257	6.43	33.74	
FeCl <sub>3</sub>	$10^{-3}$	162.2	232	6.00	2.57	0.719	1.070	3.06	32.38	

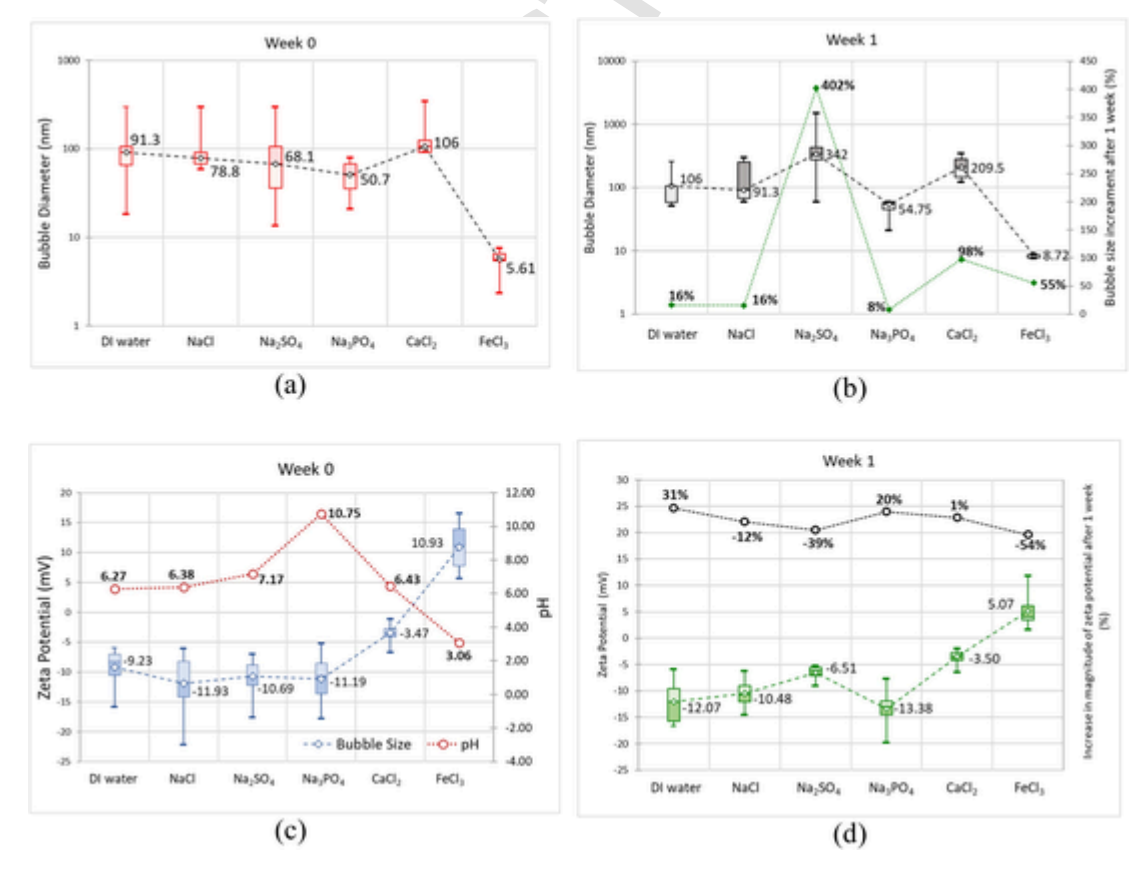


Fig. 1. The bubble size and zeta potential variation (a). bubble size at week 0, (b). bubble size, and percentage change in size after 1 week, (c). zeta potential and pH of the solution in week 0, (d). zeta potential and percentage change in zeta potential after 1 week, for air bubbles at 25 °C.

samples, and it shows the variation FeCl $_3 < DI \approx NaCl \approx CaCl_2 \leq Na_2SO_4 < Na_3PO_4$ . Between six salts samples used, Na $_3PO_4$  shows a strong alkaline condition, while FeCl $_3$  shows a strong acidic condition, which should result in highly negative zeta potential of Na $_3PO_4$  and highly positive zeta potential of FeCl $_3$  apart from their ionic valence effect.

The size of a bubble depends on three factors, the bubble breakup mechanism due to applied energy to the system, the bubble coalescence effect, and the solution properties. The energy cost for the bubble formation depends on the interfacial area and is governed by the bubble's surface tension. Higher energy is required to form smaller bubbles but lowering the surface tension at the gas/liquid interface can lower the energy requirement. Zhang et al. [22] stated that the free energy cost required ( $\Delta\Omega$ ) for the generation of bulk nanobubbles depends on three factors: (1) volume contribution, (2) interfacial energy, (3) electrostatic potential, and is given by,

$$\Delta\Omega = -\left[P_{in} - P_{out}\right]V + \gamma A + \frac{Q^2}{8\pi\epsilon R}$$
(19)

For all samples, the provided energy was identical, and condition states were similar except the salt type used, meaning the bubble size, zeta potential, and bubble concentration should wholly depend on the solution properties. In order to have a long lifespan, the bubbles should be stable against dissolution, rising over, and coalescence. Therefore, bubbles should be smaller in size to prevent rapid rise to the surface, should have lower internal pressures to prevent fast diffusion and maintain the diffusion barrier, and should have high electrical charge potentials to stop coalescence.

Nanobubbles under neutral pH have negatively charged gas-liquid interfaces (Fig. 1c and d), and the nanobubbles surface charges are believed to be a result of chemisorption of H<sub>2</sub>O, i.e., water splitting into H<sup>+</sup> and OH<sup>-</sup> during adsorption to form a hydroxylated surface [18,33,40]. OH<sup>-</sup> rather than H<sup>+</sup> is adsorbed at neutral pH conditions due to the difference in enthalpies of hydration. While the H<sup>+</sup> ions are likely to remain in the bulk aqueous phase (more likely hydrated), OHstays at the bubble gas-water interface (less likely to hydrate) [40]. The liquid water interface has a strong affinity for the electrons, and therefore nanobubbles are more likely to form in the alkaline solution. This might be the reason for stable bubbles in the Na<sub>3</sub>PO<sub>4</sub> solution which demonstrated high negative zeta potential and low percentage change in size over one week. However, when the bubbles are formed in acidic electrolyte solutions, the positive counterions are adsorbed to the bubble interface. Adsorption of positively charged ions will cause a reduction in the negativity of the charged bubbles. This effect can be reflected in the measured zeta potential values (Fig. 1c and d), where higher positively charged counterions adsorption causes smaller negative potentials. So, the CaCl2 shows a lower negative potential of approximately 3.5 mV, and FeCl<sub>3</sub> shows a positive zeta potential value of approximately 10 mV. In the FeCl<sub>3</sub> solution, the low pH value of 3.06 and the adsorption of high positive charge density Fe<sup>3+</sup> ions (232 C/mm<sup>3</sup>) to the bubble surface causes the formation of positively charged ions. In contrast, the Na<sub>3</sub>PO<sub>4</sub> solution recorded high negative zeta potentials which can be attributed to the high pH and the adsorption of OH- ions at the interface. Further, with a similar positive monovalent ion, Na+, and a similar pH range (between 6-7), the variation of zeta potential for NaCl and  $Na_2SO_4$  is influenced by the anion type, e.g.,  $Cl^-$  and  $SO_4^{2-}$ . The mobility of Cl<sup>-</sup> is higher when compared to that for SO<sub>2</sub><sup>4-</sup> and hence, the specific adsorption of Cl<sup>-</sup> at the bubble interface may be higher for the NaCl solution producing higher negative zeta potential values when compared to bubbles in Na<sub>2</sub>SO<sub>4</sub> solution.

Table 2 shows the measured and calculated results for nanobubbles in six solutions. It represents the solution type (col. 1), average bubble diameter (col.2), average bubble  $\zeta$  potential (col.3), surface charge den-

sity (col. 4), surface potential (col. 5), ionic concentration at bubble surface (col. 6), and the pressure difference ( $\Delta P$ ) (col. 7).

Fig. 2 shows the variation in surface charge density for five salt solutions, showing that magnitudes of surface charge density increase in the order of  $CaCl_2 < Na_2SO_4 < Na_3PO_4 = NaCl < FeCl_3$  at week 0 and after week 1, surface charge density decreased for all the samples except  $Na_3PO_4$ , where the surface charge density increased. As Table 1 (col E and F) shows, the ionic strength increased (and Debye length decrease) in the following order:  $NaCl < Na_2SO_4 = CaCl_2 < Na_3PO_4 = FeCl_3$ .

As shown in Fig. 3, the ionic concentration of cations at the bubble surface increases in the following order: FeCl<sub>3</sub> (Fe<sup>3+</sup>) < CaCl<sub>2</sub> (Ca<sup>2+</sup>) < Na<sub>2</sub>SO<sub>4</sub> (Na<sup>+</sup>) < NaCl (Na<sup>+</sup>) < Na<sub>3</sub>PO<sub>4</sub> (Na<sup>+</sup>) and cation concentrations were 6E-15, 1E + 03, 4E + 04, 2E + 05 and 7E + 04, times the bulk cationic concentration, respectively at week 0. After one week, the Na<sub>3</sub>PO<sub>4</sub> sample had the highest cation concentration at the bubble surface. The contact concentration of anions was increased in the following order: Na<sub>3</sub>PO<sub>4</sub> < Na<sub>2</sub>SO<sub>4</sub> < NaCl < CaCl<sub>2</sub> < FeCl<sub>3</sub> and the anion concentration was 3E-15, 5E-10, 7E-06, 3E-02, and 6E + 04 times the bulk anionic concentration, respectively.

Fig. 4 shows the variation of ion concentration with distance. Fig. 4a–e show the potential and ionic concentration distribution away from the charged bubble surface. Fig. 4f shows the potential distribution profile for all the electrolytes solutions, and Fig. 4g and h show the ion profile for cations and anions, respectively.

When monovalent Na+ counterion ions are compared in NaCl, Na<sub>2</sub>SO<sub>4</sub>, and Na<sub>3</sub>PO<sub>4</sub> solutions, they had a similar range of values of surface potentials (~11 mV) and counterion ion [Na+] concentrations at the bubble surface were 152 M, 88 M, 217 M, respectively. However, the anions (co-ions) concentrations at the surface were 7E-09 M, 5E-13 M, and 3E-18 M for Cl<sup>-</sup>, SO<sub>4</sub><sup>2-</sup> and PO<sub>4</sub><sup>3-</sup> ions, respectively and did not affect the zeta potential values. For these three samples, the potential distribution and the ion profile decayed away from the surface over the Debye length (1/K). NaCl has the highest 1/K of 9.6 nm, followed by Na<sub>2</sub>SO<sub>4</sub> (4.5 nm) and Na<sub>3</sub>PO<sub>4</sub> (2.6 nm). The results of NaCl, CaCl<sub>2</sub>, and FeCl<sub>3</sub> electrolyte solutions were compared to evaluate the impact of different valences of the counterions (cations). Here, as mentioned before, the potential distribution and ion profile decayed with the Debye length. However, as the high valency cation adsorbed to the bubble surface, there was a charge reversal. When monovalent Na+ ions and divalent  $Ca^{2+}$  ions are compared, NaCl (-11.93mV) has high negative surface potential while the  $CaCl_2$  (-3.47mV) has a lower value. The ion profiles show that NaCl solution has a high concentration of Na<sup>+</sup> ions at the surface when compared to Ca<sup>2+</sup> ions at the surface of the CaCl<sub>2</sub> solution. In both cases, the positive ion (counterion) concentration at the surface is higher than that of anions or co-ions concentration. When it comes to the FeCl<sub>3</sub> solution, the surface potential has reversed to positive (  $\sim 10$  mV). There was a very low concentration of adsorbed Fe<sup>3+</sup> ions at the bubble interface (  $\sim$  6E-18 M) compared to the anion concentration ( ~ 167 M), confirming the complete charge reversal occurs when nanobubbles adsorb Fe<sup>3+</sup> ions. When the high valency cations are bonded to the bubble surface, the negative charge on the bubble decreases. That tend to neutralize the surface charge ( $\sigma \to 0$ ,  $\psi_0 \to 0$ ). The presence of divalent ions (Ca<sup>2+</sup>), resulted in a lower magnitude negative zeta potential value around -3.5 mV. In the case of trivalent ions, Fe<sup>3+</sup>, even with very low concentrations, the bubble surface can be neutralized, and above this minimum concentration, there is charge reversal wherein the cations continue to adsorb onto the bubble surface resulting in a net positive charge.

he  $\mathrm{FeCl}_3$  solution had positive charged surface due to the solution being acidic and the adsorption of  $\mathrm{Fe}^{3+}$  ions to the bubble surface, yet the ionic concentration profile shows a very high concentration of  $\mathrm{Cl}^-$  near the bubble surface, likely causing the smaller bubble sizes. Due to the increase in negatively-charged ions that benefit from the gas-liquid

 Table 2

 The nanobubbles measured and calculated parameters.

(1)	(2)		(3)		(4)		(5)		(6)						(7)	
Solution	Average Bubble Diameter Average bubble ζ potentia		ble ζ potential	surface charge density		Surface Potential		Ionic concentration at bubble surface						Pressure Difference $(\Delta P)$		
									Cation	Anions	Total	Cation	Anions	Total		
Week	W0	W1	W0	W1	W0	W1	WO	W1	wo	W0	W0	W1	W1	W1	WO	W1
	(nm)	(nm)	(mV)	(mV)	(C/m <sup>2</sup> )	(C/m <sup>2</sup> )	(mV)	(mV)	(M)	(M)	(M)	(M)	(M)	(M)	(atm)	(atm)
H <sub>2</sub> O	91.3	106.0	-9.23	-12.07												
NaCl	78.8	91.3	-11.93	-10.48	-0.0011	-0.0009	-12.49	-10.95	1.52E + 02	6.59E-09	152.00	3.56E + 01	2.81E-08	35.60	35.96	31.06
Na <sub>2</sub> SO <sub>4</sub>	68.1	342.0	-10.69	-6.51	-0.0010	-0.0005	-11.17	-6.77	8.78E + 01	5.19E-13	87.80	1.34E + 00	2.22E-09	1.34	41.66	8.29
Na <sub>3</sub> PO <sub>4</sub>	50.7	54.8	-11.19	-13.38	-0.0011	-0.0013	-11.73	-14.05	2.17E + 02	2.64E-18	217.00	1.94E + 03	3.71E-21	1940.00	55.96	51.72
CaCl <sub>2</sub>	106	209.5	-3.47	-3.50	-0.0003	-0.0003	-3.64	-3.66	1.03E + 00	6.23E-05	1.03	1.10E + 00	6.04E-05	1.10	26.81	13.56
FeCl <sub>3</sub>	5.6	8.7	+10.93	+5.07	0.0014	0.0006	12.73	5.78	5.76E-18	1.67E + 02	167.00	2.47E-10	4.78E-01	0.48	507.38	326.68

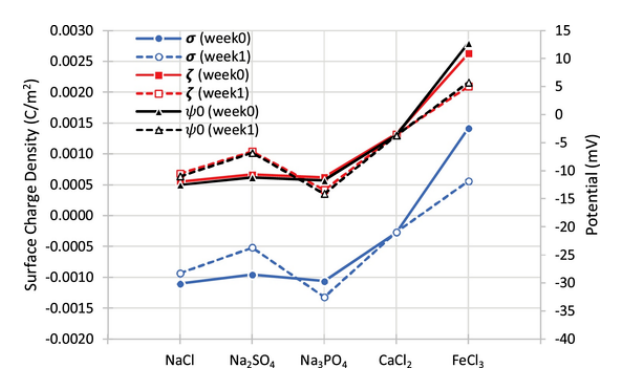


Fig. 2. Surface charge density, zeta potential and surface potential at week 0 and week 1.

interface may lead to an increase of the electrostatic repulsion force between the nanobubbles and surface, resulting in a decrease in the average diameter of nanobubbles [41]. For five electrolyte solutions (excluding FeCl<sub>3</sub>), the surface charge density and the anion attraction were inversely proportional. This explains that the bubbles with high surface charge density (negatively charged bubble) tend to repel the like-charged anions away from the surface that resulted in a low concentration of anions at the surface. As the results indicate, at the gas-liquid interface, there was a high charge density of ions which can act as "structure-makers" in aqueous solution [42,43]. These ionic impurities form a diffusive shield to the outflux of gases making the bubbles more stable, and at the same time, lower the effective value of the liquid-gas surface tension [44]. Further, the ionic impurities are adsorbed at the gas-liquid interface resulting in mutual repulsion between the ions and also resulting change in surface tension will result in reducing the internal gas pressure and prevention the fast gas diffusion [44].

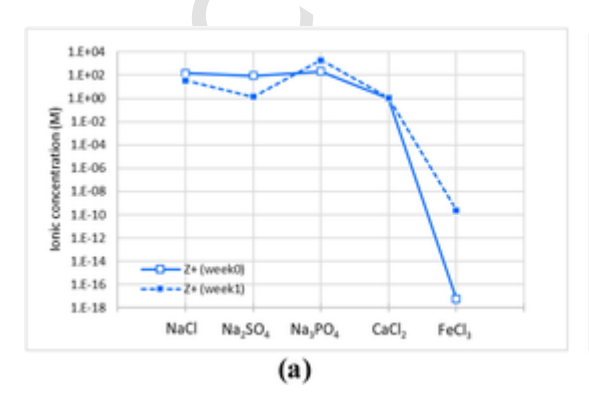
Inorganic ions can interact with the charged surface in either non-specific ion adsorption or specific ion adsorption. As all the graphs show, for all cases, ions are adsorbed onto the bubble surface, as their concentration is higher than the bulk concentration. It is therefore assumed that one mode of nanobubble stability depends on the ion adoption at the gas-liquid interface called the ionic shielding effect [42,45]. All the electrolyte solutions had the same low ionic bulk concentration of 0.001 M, and the results indicate that all the samples were relatively stable over time. This can be attributed to the presence of relatively high Debye length, and firmly adsorbed ions at the gas-liquid interface. This will result in reducing bubble coalescence as well as gas diffusion, thereby increasing the bubble stability.

Table 2 (col.7) shows the pressure difference calculated for each solution based on Eq. (18). All the results were calculated with the assumption that surface tension values are equal to 0.072 N/m, the surface tension of the water at 20 °C. Results indicated that the calculated pressure differences are very high and increase in the order of CaCl<sub>2</sub> (26.81 atm) < NaCl (35.96 atm) < Na<sub>2</sub>SO<sub>4</sub> (41.66 atm) < Na<sub>3</sub>PO<sub>4</sub>

(55.96 atm)  $\leq$  FeCl<sub>3</sub> (507.38 atm). At these high pressures, it is unlikely the bubble would be stable, suggesting that the actual surface tension may be significantly lower than that of water at 20 °C. Hence, a change in the interfacial properties of the bubble likely have occurred, reducing the surface tension at the gas-liquid interface. This possibility of reduction in surface tension has been addressed by others. Ushida et al. [46] stated that solutions containing large concentrations of nanobubbles could reduce the surface tension by 15 % and Attard [47] explained that surface tension reduces due to supersaturation and hence reduces the pressure. Further Das et al. [44] and Uchida et al. [42] explained that the ion impurities act as a diffusion shield at the gas-liquid interface, increasing the stability against gas outflux and could lower the effective value of the gas-liquid surface tension.

The bulk electrolyte ion concentration has a significant contribution not only to the electrostatic potential but also to the forces between charged surfaces. DLVO theory explains that the stability of the colloidal system depends on the force or energy balance between the van der Waals attractive interaction and the electrical double layer interaction. This theory explains that an energy barrier resulting from repulsive forces or energy would prevent the two particles from approaching each other and coalescing. Accordingly, Fig. 5 presents the attractive, repulsive, and total interacting forces/energy diagrams for five electrolyte bubble solutions. Since the recorded results had very low electrical charges (low zeta potential values), the attractive van der Waals forces dominated. In the case of the NaCl solution, we can see an energy barrier of  $1.87 \times 10^{-20} J$  at a 5 nm separation distance. For the samples of Na<sub>2</sub>SO<sub>4</sub>, Na<sub>3</sub>PO<sub>4</sub>, CaCl<sub>2</sub>, and FeCl<sub>3</sub>, there was no energy barrier to prevent bubble coalescence based on the DLVO calculations.

The above results indicate that the instability of the nanobubble systems for Na<sub>2</sub>SO<sub>4</sub>, Na<sub>3</sub>PO<sub>4</sub> CaCl<sub>2</sub> and FeCl<sub>3</sub> solutions based on the high net attractive forces compared to the repulsive forces. Fig. 6 shows the comparison of electric double layer and van der Waals interaction potentials for two salt solutions of similar Debye lengths. Fig. 6a shows the electric double layer repulsion force is higher for the Na2SO4 (a = 34 nm,  $\zeta = -6.51$  mV,  $n_{total}(r = a + d) = 88$  M) when compared to that for CaCl<sub>2</sub> (a = 53 nm,  $\zeta = -3.50$  mV,  $n_{total}(r = a + d) = 1$  M). Also, van der Waals attraction potential is higher for CaCl2 due to large bubble size. Fig. 6b shows that Na<sub>3</sub>PO<sub>4</sub> (a = 25.35 nm,  $\zeta$ =-11.19 mV,  $n_{total}(r = a + d) = 217 \text{ M}$ ) has higher electrical repulsion potential compared to that for FeCl<sub>3</sub> (a = 2.8 nm,  $\zeta = +10.93$  mV,  $n_{total}(r = a + d)$ = 167 M). However, since the bubbles in FeCl<sub>3</sub> solution were much smaller, as it has a comparatively smaller van der Waals attraction potential. Therefore, with similar Debye lengths, electric double layer repulsion potential of nanobubbles will be depend on the surface/zeta potential and adsorbed ion type and ion concentration at the surface. Also the monovalent ion adsorption will be beneficial towards the electrostatic repulsion and related bubble stability. However, bubble size is key factor when discussing the total interaction force/potential as for



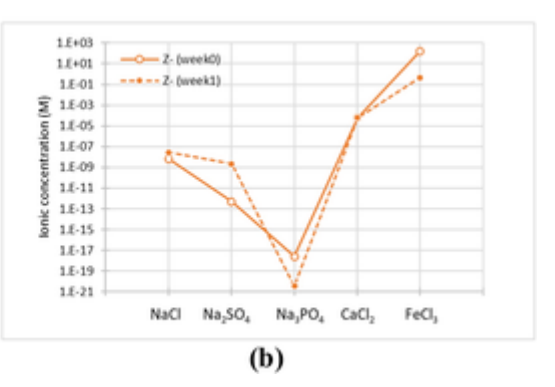


Fig. 3. Ionic concentration at the bubble surface for different salts (a). cation (b). anions.

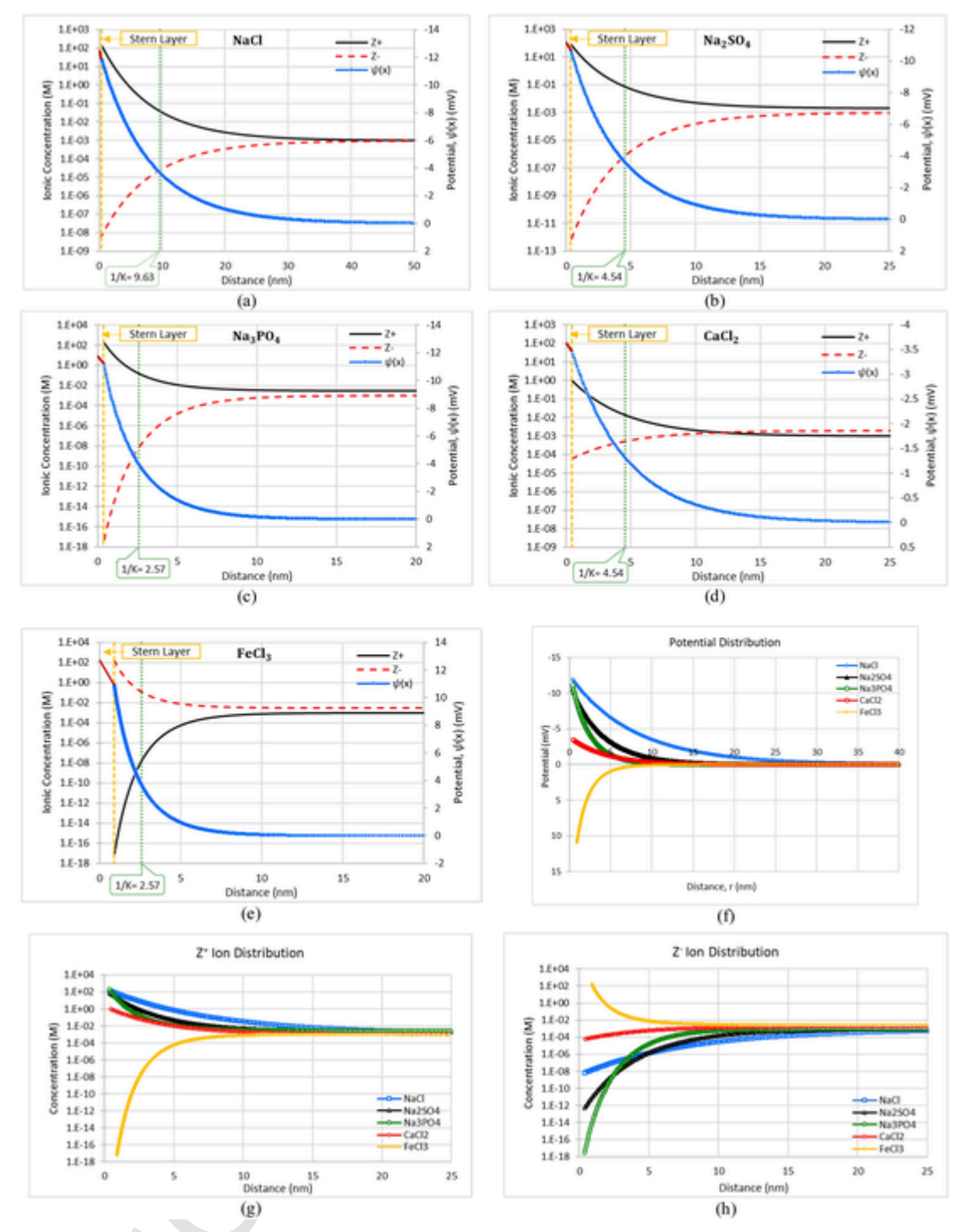


Fig. 4. The variation of ion concentration with distance.

larger bubbles attractive forces are always impacted at smaller separation distances. For all the four samples shown in Fig. 6, for separation distances smaller than the Debye length, the van der Waals attraction potential is very much higher and therefore, the total interaction potential governed by the attractive force.

The experimental results indicated long term stability of these nanobubbles for all the five electrolytes solutions. One of the main concerns for deviation may be the Hamaker's constant used for the calculation of van der Waals forces. As we are still not certain of the exact properties of the bubble interface, values used for computation may be overestimated. Takahashi [40] explains that the  $\rm H^+$  and  $\rm OH^-$  ions have

an exclusive effect on the gas-water interface electrical charge. These ions are essential for the hydrogen bond network at the gas-liquid interface, and the hydrogen bond structure at the interface differs from the bulk solution as do the density, viscosity, electrical conductivity, and dielectric permittivity.

Ohgaki et al. [48] showed the possibility of highly structured hydrogen bonds at the gas-liquid interface of nanobubble that enhance bubble stability. Also, with the accumulation of ion impurities, a possible of "structure-maker" at the bubble interface can act as a shield [44,49]. In such a hard-interfacial structure, the assumed Hamaker constant might not be valid and may lead to erroneous conclusions.

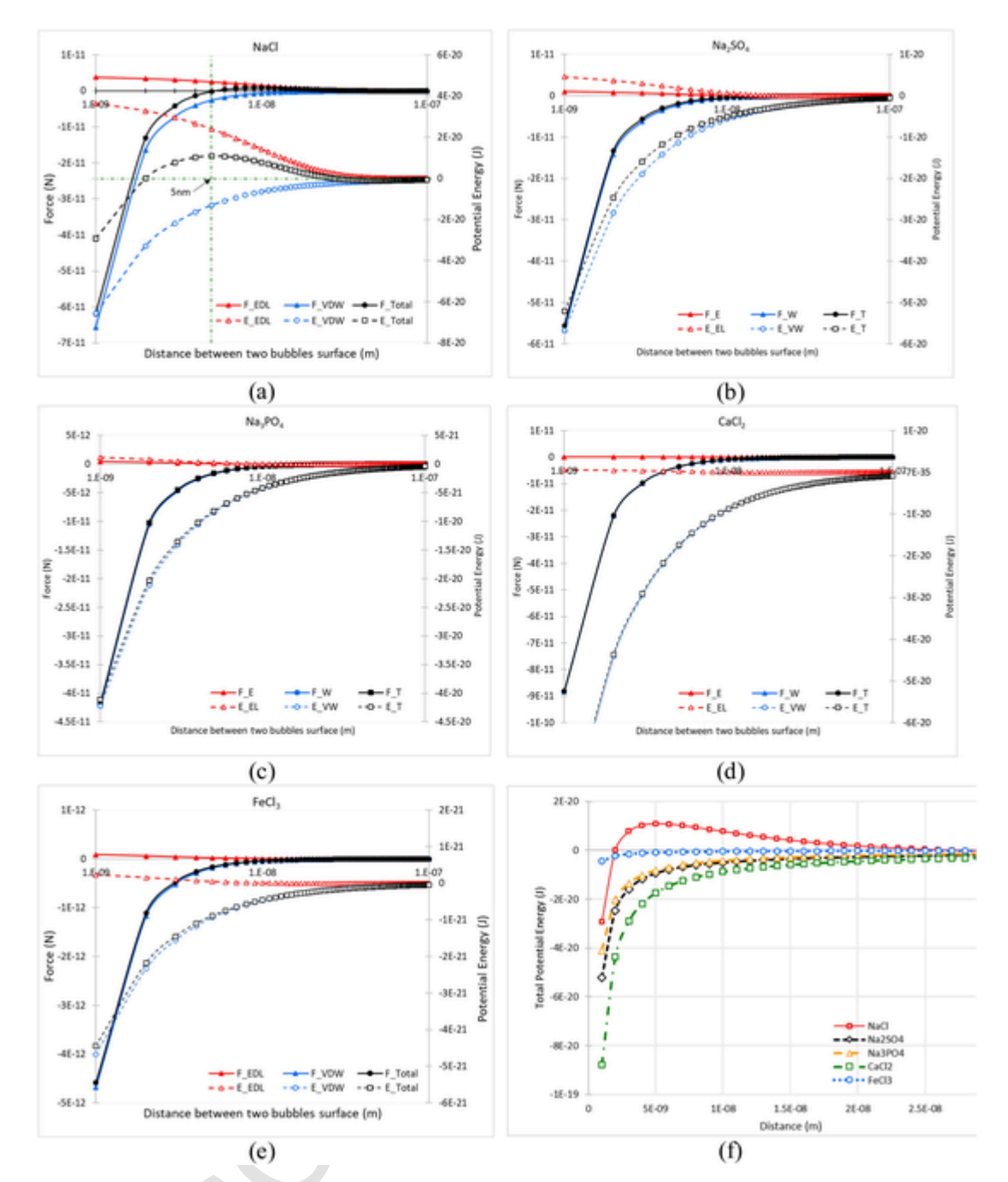


Fig. 5. The attractive, repulsive, and total interacting forces/energy diagrams for five electrolyte bubble solutions.

Further, it should be noted that, as two bubbles approach each other, the thin film between them has higher salt concentrations than that in the bulk fluid, and there may be weakened van der Waals forces, and hence the calculation of Hamaker constants may require further modifications. Depending on the ion type, both  $\sigma$  and  $\Psi_0$  can change leading to a substantial reduction in the repulsive double-layer forces.

Table 3 summarizes findings for the nanobubble formation in different valency electrolytes. Those findings are consistent with the experimental results presented here. In summary, nanobubbles in pure water are negatively charged, and with increased concentration of electrolyte, the magnitude of the zeta potential decreases. Nanobubbles were negatively charged with the monovalent electrolytes, and with the increased cation valency, the zeta potential is neutralized or completely reversed. In literature, this phenomenon was explained with re-

spect to the specific cation ion adsorption or in high pH conditions, the adsorption of cation hydroxides on the gas-liquid interface of the bubble. However, the published literature does not discuss the long-term stability or application of DLVO theory to nanobubbles for multivalent electrolytes. Therefore, the present research attempts to fulfill this research gap.

#### 7. Summary and conclusions

All electrolytes solutions with 0.001 M concentration produced stable bubbles over one week, with no significant deviation in either bubble size or zeta potential values. The difference between the bubble size and zeta potential can be attributed to the solution properties and mainly dependent on solution pH and the cation valency, as nanobubbles under natural pH solutions tend to be negatively charged. Anions

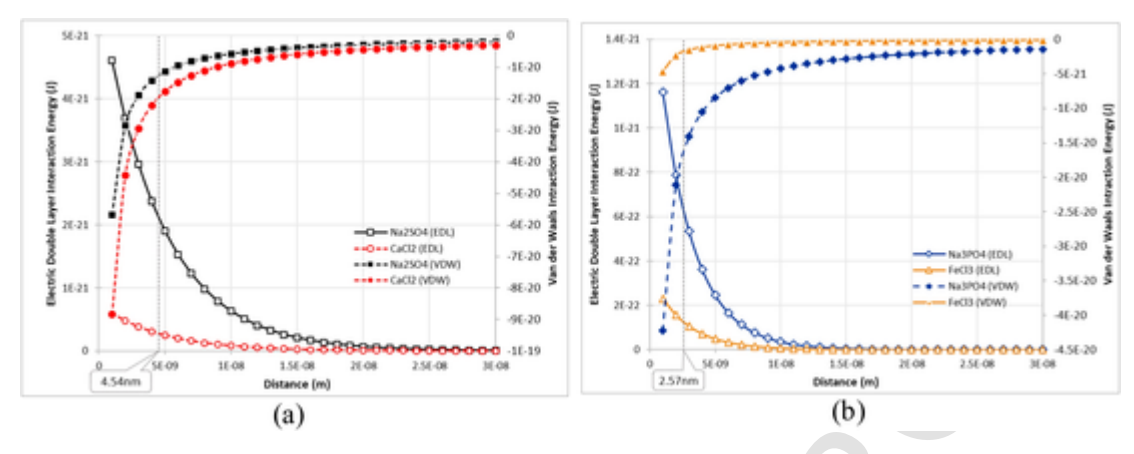


Fig. 6. Comparison of results of salts solutions with similar Debye lengths (a). 1/K = 4.54 nm Na<sub>2</sub>SO<sub>4</sub> and CaCl<sub>2</sub>, (b). 1/K = 2.57 nm Na<sub>3</sub>PO<sub>4</sub> and FeCl<sub>3</sub>.

had minimal impact on the surface potential. The ion profiles revealed that cation concentrations at the bubble surface were higher than that of bulk liquid, confirming that the bubbles are negatively charged for neutral and high pH values ( $\geq$  4) for low valency cation adsorption. Low adsorption of high valency cations neutralized the charge on the bubble surface or completely reversed the charge. However, low ionic adsorptions at the gas-liquid interface produced stable nanobubbles due to the ion shielding effects. Also, with stable bubbles, the calculation of the attractive van der Waals forces produced unrealistic values suggesting that the Hamaker constant used for the calculation may not be valid at the nanobubble gas-liquid interface. Further, calculated pressure values were also unrealistically elevated and suggest that surface tension values should be lower than that of the surface tension of water. These results revealed that nanobubbles should contain exceptional interfacial properties that need to be carefully investigated and evaluated.

#### CRediT authorship contribution statement

Shaini Aluthgun Hewage: Conceptualization, Methodology, Validation, Formal analysis, Investigation, Data curation, Writing - original draft, Writing - review & editing, Visualization. Jitendra Kewalramani: Methodology, Investigation. Jay N. Meegoda: Conceptualization, Methodology, Resources, Writing - review & editing, Supervision, Project administration, Funding acquisition.

# **Declaration of Competing Interest**

The authors report no declarations of interest.

# Acknowledgments

This research was sponsored by the US National Science Foundation Award #1634857 entitled "Remediation of Contaminated Sediments with Ultrasound and Ozone Nanobubbles."

 ${\bf Table~3}$  The summary of findings for the nanobubbles in multivalent electrolytes from the published literature.

#	Author (Year)	Bubble Generation Method	Gas Type	Electrolytes	Findings			
	()		-7F-		Conclusions	Condition	Average bubble size at pH (5.5–7) and 25° C	Average, Zeta potential at pH (5.5–7) and 25° C
1	Nirmalkar et al (2018) [50]	hydrodynamic cavitation	Air	NaCl, CaI <sub>2</sub> , AlCl <sub>3</sub>	The addition of any salt leads to a reduction in bubble number density and a rise in the mean bubble diameter. The magnitude of the negative zeta potential decreases with added NaCl and Cal <sub>2</sub> , neutralizing the bubble charge while AlCl <sub>3</sub> reverses to a positive potential. Beyond the critical concentration of salts, the bubble system becomes unstable. The DLVO theory calculation for pure water shows the stable colloidal system for bulk nanobubbles.	NaCl (0.001 M) CaI <sub>2</sub> (0.001 M) AlCl <sub>3</sub> (0.001 M)	100 150 125	-28.0-24.0- 4.0
2	Sjogreen et al(2018) [51]	Injection of oxygen to a saline solution in a diffusive medium	$O_2$	NaCl	The highest stability of nanobubbles obtained at the temperature $T=4^{\circ}C$ with the diameter of the nanobubbles remains approximately constant with time, in the 0.9% NaCl concentration, irrespective of pH values.	NaCl (0.9 %)	588	-13.1
3	Yurchenko et al (2016) [52]	optical (laser- Induced) breakdown	Air	KI, NaI, NaClO <sub>3</sub> , CaCl <sub>2</sub> , MaCl <sub>2</sub> , KBr, NaBr, KCl, NaCl, NaNO <sub>3</sub> , CsCl	They studied the bubstons, the stable bubble formation in electrolyte solutions with the ionic. They concluded nanobubbles stabilized by adsorption of chaotropic anions at the gas-liquid interface and the impact of cosmotropic cations is weak adsorption.	NaCl (0.1 M) CaCl <sub>2</sub> (0.1 M) Na <sub>2</sub> SO <sub>4</sub> (0.1 M)	250 370 190	_
4	Jia et al (2013) [53]	bubble nucleation in a gas- supersaturated solution	Air	KCl	The pH of the solution greatly influences the bubbles zeta potential and should be well considered on the flotation process. The positive ions (H <sup>+</sup> ) favorably remain in the bulk aqueous phase allowing negative ions to be adsorbed at the gas-liquid interface. As pH decreases, OH <sup>-</sup> concentration decreases and potentially causing charge reversal and forming positively charged bubbles.	KCl (0.001 M)	-	-5.8
5	Leroy et al. (2012) [54]	Theoretical work. Values used from the previous literature	Vapor	NaCl, KCl	They have developed the surface complex model for the gas/ water interface by considering the negative surface sites and used to (I) determine the true values of zeta potential for H <sub>2</sub> bubbles in NaCl solution, (II) correct the electrophoretic mobility of H <sub>2</sub> bubbles from the retardation effect of surface conductivity, (III) predict the surface tension of the air/KCl solution interface.	NaCl (0.001 M)	-	<b>-32.5</b>
6	Bunkin et al (2012) [55]	Spontaneous gas cavities (bubstons)	Air	NaCl	Three independent techniques (phase microscopy, DLS, and polarimetric scatterometry) were used to claim the long-living gas nanobubble clusters in an aqueous salt solution with saturated dissolved gas.	-	-	-
7	Najafi et al (2007) [56]	Bubble nucleation	Air	NaCl, CaCl <sub>2</sub> , Al <sub>2</sub> (SO4) <sub>3</sub>	Nanobubbles in an electrolyte solution, based on the valency of the cation and its concentration, the zeta potential reduced, neutralized, or even reverse the charge.	NaCl (0.001 M) CaCl <sub>2</sub> (0.001 M) Al <sub>2</sub> (SO <sub>4</sub> ) <sub>3</sub> (0.001 M)	*Background 0.0001 M SDS solution	-70.7- 28.5 +3.6
8	Han et al. (2006) [57]	Electrochemical reaction	O <sub>2</sub> , H <sub>2</sub>	NaCl KCl MgCl <sub>2</sub> CaCl <sub>2</sub> AlCl <sub>3</sub>	The zeta potential was measured in various electrolyte solutions. Nanobubbles were negatively charged for Na $^+,$ K $^+,$ and Ca $^{2+}$ at every concentration and pH range. However, the magnitude of the zeta potential decreased with an increase in concentration and a decrease in pH value. Positive nanobubbles were recorded for concentrations higher than the critical concentration of Mg $^{2+}$ for $10^{-2}\mathrm{M}$ and Al $^{3+}$ for $10^{-5}$ M. They conclude that the generation of positively charged bubbles is attributed to both specific adsorptions of hydroxylated species and precipitation of metal hydroxides on the bubble interface.	NaCl (0.01 M) KCl (0.01 M) *MgCl <sub>2</sub> (0.001 M) *CaCl <sub>2</sub> (0.001 M) *AlCl <sub>3</sub> (0.001 M)	*Background 0.01 NaCl	-30-33-20- 40 +25

#	Author (Year)	Bubble Generation Method	Gas Type	Electrolytes	Findings			
					Conclusions	Condition	Average bubble size at pH (5.5–7) and 25° C	Average, Zeta potential at pH (5.5–7) and 25° C
9	Han et al. (2006) [58]	Electrochemical reaction	O <sub>2</sub> , H <sub>2</sub>	AlCl <sub>3</sub>	The positively charged bubbles were formed by controlling the aluminum concentration and pH. Bubbles zeta potentials were positive at pH 3–7 for both 10 $^{-3}$ and 10 $^{-4}$ M AlCl $_3$ solutions. The charge reversal of bubbles influenced by the	*AlCl <sub>3</sub> (0.001 M)	*Background 0.01 NaCl	+25
10	Takahashi (2005) [40]	Hydrodynamic cavitation	Air	NaCl MgCl <sub>2</sub>	hydrated precipitation of positively charged Al species, and Al <sup>3+</sup> , Al(OH) <sub>3</sub> (s), and Al(OH) <sub>4</sub> - was the predominant species. For a wide range of pH conditions, microbubbles were negatively charged and positive under strongly acidic conditions. In the inorganic electrolytes solutions, zeta potential decreases by increasing the number of counterions within the slipping plane. OH <sup>-</sup> and H <sup>+</sup> ions dominate the charging mechanism of the gas-water interface, while other anions and cations have secondary effects. The force of the attraction depends on the valency of the counterions, and ions	NaCl (0.001 M) MgCl <sub>2</sub> (0.001 M)	-	-23.0- 14.0
11	Cho et al (2005) [59]	Sonicated with a palladium electrode		NaCl, CaCl <sub>2</sub> , Na <sub>2</sub> SO <sub>4</sub>	with high valency attract to the interface more strongly. The zeta-potentials of nanobubbles increase with salt concentrations. Generally, nanobubbles have negatively charged surface; hence increase in electrolyte concentration allows more cation adsorption and compresses the electrical double layer thickness of a bubble. Compared to NaCl, with the presence of bivalent cations, Ca <sup>2+</sup> in CaCl <sub>2</sub> solution cause less negative zeta potential. Further suggesting that the bubble charge would be influenced by anion type between Cl <sup>-</sup> and	NaCl (0.001 M) Na <sub>2</sub> SO <sub>4</sub> (0.001 M) CaCl <sub>2</sub> (0.001 M)	850 853 850	-14.5-10.9- 7.5
12	Han et al. (2004) [60]	Electrochemical reaction	O <sub>2</sub> , H <sub>2</sub>	MgCl <sub>2</sub> CaCl <sub>2</sub>	SO <sub>4</sub> <sup>2-</sup> . The bubbles were negatively charged for CaCl <sub>2</sub> in all range of concentration and pH conditions, and the charge reversal of bubbles found in MgCl <sub>2</sub> in certain circumstances. Mg <sup>2+</sup> formed positively charged nanobubbles above 10 <sup>-2</sup> M concentration and above pH 9. The charge reversal explained as the combined mechanism of both specific adsorptions of hydroxylated species and the formation of hydroxide precipitates.	*MgCl <sub>2</sub> (0.001 M) *CaCl <sub>2</sub> (0.001 M)	*Background 0.01 NaCl	-20- 40
13	Karraker and Radke (2002) [61]	Porous-plate technique	Air	NaCl, KClO <sub>3</sub> , K <sub>2</sub> SO <sub>4</sub> , CaCl <sub>2</sub>	There is no influence of changing the electrolyte to NaCl or KClO <sub>3</sub> on the disjoining pressure isotherms. However, between CaCl <sub>2</sub> and K <sub>2</sub> SO <sub>4</sub> solutions with similar Debye length, the equilibrium film thickness is smaller for the CaCl <sub>2</sub> , suggesting that the gas-liquid interface is negatively charged and hence the divalent Ca <sup>2+</sup> screen the charge more effectively	NaCl (0.01 M)	-	-38.0
14	Yang et al (2001) [62]	electrophoresis	H <sub>2</sub>	NaCl, CaCl <sub>2</sub> , AlCl <sub>3</sub>	compared to K <sup>+</sup> univalent ions. In univalent NaCl solutions, bubbles were negatively charged, but with the presence of multivalent metal ions magnitude of the zeta potential can be significantly changed, even reverse the bubble's charge polarity.	NaCl (0.001 M) NaCl (0.01 M) *CaCl <sub>2</sub> (0.001 M) *AlCl3 (0.001 M)	*Background 0.01 NaCl	-35.0-26.0- 5.5 +12.0

#### References

- A. Agarwal, W.J. Ng, Y. Liu, Principle and applications of microbubble and nanobubble technology for water treatment, Chemosphere (2011), doi:10.1016/ j.chemosphere.2011.05.054.
- [2] K. Ebina, K. Shi, M. Hirao, J. Hashimoto, Y. Kawato, S. Kaneshiro, T. Morimoto, K. Koizumi, H. Yoshikawa, Oxygen and air nanobubble water solution promote the growth of plants, fishes, and mice, PLoS One (2013), doi:10.1371/journal.pone.0065339.
- [3] N. Nirmalkar, A.W. Pacek, M. Barigou, On the existence and stability of bulk nanobubbles, Langmuir 34 (2018) 10964–10973, doi:10.1021/ acs.langmuir.8b01163.
- [4] A.J. Jadhav, M. Barigou, Bulk nanobubbles or not nanobubbles: that is the question, Langmuir (2020), doi:10.1021/acs.langmuir.9b03532.
- [5] F.Y. Ushikubo, T. Furukawa, R. Nakagawa, M. Enari, Y. Makino, Y. Kawagoe, T. Shiina, S. Oshita, Evidence of the existence and the stability of nano-bubbles in water, Colloids Surf. A Physicochem. Eng. Asp. 361 (2010) 31–37, doi:10.1016/j.colsurfa.2010.03.005.

- [6] S. Liu, Y. Kawagoe, Y. Makino, S. Oshita, Effects of nanobubbles on the physicochemical properties of water: the basis for peculiar properties of water containing nanobubbles, Chem. Eng. Sci. (2013), doi:10.1016/j.ces.2013.02.004.
- [7] H. Li, L. Hu, D. Song, F. Lin, Characteristics of micro-nano bubbles and potential application in groundwater bioremediation, Water Environ. Res. (2015), doi:10.2175/106143014x14062131177953.
- [8] L. Hu, Z. Xia, Application of ozone micro-nano-bubbles to groundwater remediation, J. Hazard. Mater. (2018), doi:10.1016/j.jhazmat.2017.08.030.
- [9] Z. Xia, L. Hu, Treatment of organics contaminated wastewater by ozone micro-nano-bubbles, Water (Switzerland) (2018), doi:10.3390/w11010055.
- [10] J.H. Batagoda, S.D.A. Hewage, J.N. Meegoda, Nano-ozone bubbles for drinking water treatment, J. Environ. Eng. Sci. 14 (2019) 57–66, doi:10.1680/ jenes.18.00015.
- [11] J.N. Meegoda, J.H. Batagoda, S. Aluthgun-Hewage, Briefing: in situ decontamination of sediments using ozone nanobubbles and ultrasound, J. Environ. Eng. Sci. 12 (2017), doi:10.1680/jenes.17.00006.
- [12] J.H.J.H. Batagoda, J.N.J.N. Meegoda, S.A. Hewage, S. Aluthgun-hewage, In situ remediation of passaic river sediments using ultrasound and ozone nanobubbles, world environ, Water Resour. Congr. 2018 (2018) 49–63, doi:10.1061/ 9780784481417.005.

- [13] J.H. Batagoda, S. Aluthgun Hewage, J.N. Meegoda, Remediation of heavy-metal-contaminated sediments in USA using ultrasound and ozone nanobubbles, J. Environ. Eng. Sci. (2019), doi:10.1680/jenes.18.00012.
- [14] S. Aluthgun Hewage, J.H. Batagoda, J.N. Meegoda, In situ remediation of sediments contaminated with organic pollutants using ultrasound and ozone nanobubbles, Environ. Eng. Sci. (2020) ees.2019.0497, doi:10.1089/ ees.2019.0497.
- [15] Y. Gao, C. Hernandez, H.X. Yuan, J. Lilly, P. Kota, H. Zhou, H. Wu, A.A. Exner, Ultrasound molecular imaging of ovarian cancer with CA-125 targeted nanobubble contrast agents, nanomedicine nanotechnology, Biol. Med. (2017), doi:10.1016/j.nano.2017.06.001.
- [16] E.Y. Lukianova-Hleb, X. Ren, R.R. Sawant, X. Wu, V.P. Torchilin, D.O. Lapotko, On-demand intracellular amplification of chemoradiation with cancer-specific plasmonic nanobubbles, Nat. Med. (2014), doi:10.1038/nm.3484.
- [17] S.S. Thakur, Y.S. Chen, Z.H. Houston, N. Fletcher, N.L. Barnett, K.J. Thurecht, I.D. Rupenthal, H.S. Parekh, Ultrasound-responsive nanobubbles for enhanced intravitreal drug migration: an ex vivo evaluation, Eur. J. Pharm. Biopharm. (2019), doi:10.1016/j.ejpb.2019.01.014.
- [18] J.N. Meegoda, S. Aluthgun Hewage, J.H. Batagoda, Stability of nanobubbles, Environ. Eng. Sci. 35 (2018), doi:10.1089/ees.2018.0203.
- [19] A. Azevedo, H. Oliveira, J. Rubio, Bulk nanobubbles in the mineral and environmental areas: updating research and applications, Adv. Colloid Interface Sci. (2019), doi:10.1016/j.cis.2019.101992.
- [20] H.H. Sang, X.Y. Jiao, S.F. Wang, W.H. Guo, M.K. Salahou, K.H. Liu, Effects of micro-nano bubble aerated irrigation and nitrogen fertilizer level on tillering, nitrogen uptake and utilization of early rice, Plant Soil Environ. (2018), doi:10.17221/240/2018-PSE.
- [21] S. Calgaroto, K.Q. Wilberg, J. Rubio, On the nanobubbles interfacial properties and future applications in flotation, Miner. Eng. 60 (2014) 33–40, doi:10.1016/ j.mineng.2014.02.002.
- [22] X.Y. Zhang, Q.S. Wang, Z.X. Wu, D.P. Tao, An experimental study on size distribution and zeta potential of bulk cavitation nanobubbles, Int. J. Miner. Metall. Mater. (2020), doi:10.1007/s12613-019-1936-0.
- [23] T. Temesgen, T.T. Bui, M. Han, T. il Kim, H. Park, Micro and nanobubble technologies as a new horizon for water-treatment techniques: a review, Adv. Colloid Interface Sci. (2017), doi:10.1016/j.cis.2017.06.011.
- [24] C. Chen, J. Li, X. Zhang, The existence and stability of bulk nanobubbles: a long-standing dispute on the experimentally observed mesoscopic inhomogeneities in aqueous solutions, Commun. Theor. Phys. 72 (2020) 037601, doi:10.1088/1572-9494/ab6183.
- [25] Y. Sun, G. Xie, Y. Peng, W. Xia, J. Sha, Stability theories of nanobubbles at solid-liquid interface: a review, Colloids Surf. A Physicochem. Eng. Asp. (2016), doi:10.1016/j.colsurfa.2016.01.050.
- [26] T.T. Bui, D.C. Nguyen, M. Han, Average size and zeta potential of nanobubbles in different reagent solutions, J. Nanoparticle Res. (2019), doi:10.1007/ s11051-019-4618-y.
- [27] Z. Guo, X. Wang, H. Wang, B. Hu, Z. Lei, M. Kobayashi, Y. Adachi, K. Shimizu, Z. Zhang, Effects of nanobubble water on the growth of: Lactobacillus acidophilus 1028 and its lactic acid production, RSC Adv. (2019), doi:10.1039/c9ra05868k.
- [28] A. Khaled Abdella Ahmed, C. Sun, L. Hua, Z. Zhang, Y. Zhang, T. Marhaba, W. Zhang, Colloidal properties of air, oxygen, and nitrogen nanobubbles in water: effects of ionic strength, natural organic matters, and surfactants, Environ. Eng. Sci. 35 (2018) 720–727, doi:10.1089/ees.2017.0377.
- [29] A.J. Jadhav, M. Barigou, Proving and interpreting the spontaneous formation of bulk nanobubbles in aqueous organic solvent solutions: effects of solvent type and content, Soft Matter. (2020), doi:10.1039/d0sm00111b.
- [30] K. Yasuda, H. Matsushima, Y. Asakura, Generation and reduction of bulk nanobubbles by ultrasonic irradiation, Chem. Eng. Sci. 195 (2019) 455–461, doi:10.1016/j.ces.2018.09.044.
- [31] S.H. Min, M.L. Berkowitz, Bubbles in water under stretch-induced cavitation, J. Chem. Phys. 150 (2019) 054501, doi:10.1063/1.5079735.
- [32] S. Kim, H. Kim, M. Han, T. Kim, Generation of sub-micron (nano) bubbles and characterization of their fundamental properties, Environ. Eng. Res. 24 (2018) 382–388, doi:10.4491/eer.2018.210.
- [33] J.N. Meegoda, S.A. Hewage, J.H. Batagoda, Application of the diffused double layer theory to nanobubbles, Langmuir (2019), doi:10.1021/ acs.langmuir.9b01443.
- [34] J.J. López-García, A.A. Moya, J. Horno, A. Delgado, F. González-Caballero, A network model of the electrical double layer around a colloid particle, J. Colloid Interface Sci. 183 (1996) 124–130, doi:10.1006/jcis.1996.0525.
- [35] F.L. Leite, C.C. Bueno, A.L. Da Róz, E.C. Ziemath, O.N. Oliveira, Theoretical models for surface forces and adhesion and their measurement using atomic force microscopy, Int. J. Mol. Sci. (2012), doi:10.3390/ijms131012773.
- [36] V. Uskoković, Dynamic light scattering based microelectrophoresis: main prospects and limitations, J. Dispers. Sci. Technol. (2012), doi:10.1080/ 01932691.2011.625523.

- [37] J.N. Israelachvili, Electrostatic forces between surfaces in liquids, Intermol. Surf. Forces, 2011, doi:10.1016/b978-0-12-375182-9.10014-4.
- [38] M.J. Prince, H.W. Blanch, Transition electrolyte concentrations for bubble coalescence, AIChE J. (1990), doi:10.1002/aic.690360915.
- [39] M. Firouzi, T. Howes, A.V. Nguyen, A quantitative review of the transition salt concentration for inhibiting bubble coalescence, Adv. Colloid Interface Sci. (2015), doi:10.1016/j.cis.2014.07.005.
- [40] M. Takahashi, ζ potential of microbubbles in aqueous solutions: electrical properties of the gas - water interface, J. Phys. Chem. B. (2005), doi:10.1021/ jp0445270.
- [41] B. Bhushan, Y. Pan, S. Daniels, AFM characterization of nanobubble formation and slip condition in oxygenated and electrokinetically altered fluids, J. Colloid Interface Sci. 392 (2013) 105–116, doi:10.1016/j.jcis.2012.09.077.
- [42] T. Uchida, S. Liu, M. Enari, S. Oshita, K. Yamazaki, K. Gohara, Effect of NaCl on the lifetime of micro- and nanobubbles, Nanomaterials 6 (2016) 31, doi:10.3390/ nano6020031.
- [43] T. Corridoni, R. Mancinelli, M.A. Ricci, F. Bruni, Viscosity of aqueous solutions and local microscopic structure, J. Phys. Chem. B 115 (2011) 14008–14013, doi:10.1021/jp202755u.
- [44] S. Das, J.H. Snoeijer, D. Lohse, Effect of impurities in description of surface nanobubbles, Phys. Rev. E 82 (2010) 056310, doi:10.1103/PhysRevE.82.056310.
- [45] E. Dressaire, R. Bee, D.C. Bell, A. Lips, H.A. Stone, Interfacial polygonal nanopatterning of stable microbubbles, Science (80-) (2008), doi:10.1126/ science.1154601.
- [46] A. Ushida, T. Hasegawa, T. Narumi, T. Nakajima, Flow properties of nanobubble mixtures passing through micro-orifices, Int. J. Heat Fluid Flow 40 (2013) 106–115, doi:10.1016/j.ijheatfluidflow.2013.01.013.
- [47] P. Attard, The stability of nanobubbles, Eur. Phys. J. Spec. Top. (2013), doi:10.1140/epjst/e2013-01817-0.
- [48] K. Ohgaki, N.Q. Khanh, Y. Joden, A. Tsuji, T. Nakagawa, Physicochemical approach to nanobubble solutions, Chem. Eng. Sci. 65 (2010) 1296–1300, doi:10.1016/j.ces.2009.10.003.
- [49] J.H. Weijs, J.R.T. Seddon, D. Lohse, Diffusive shielding stabilizes bulk nanobubble clusters, ChemPhysChem (2012), doi:10.1002/cphc.201100807.
- [50] N. Nirmalkar, A.W. Pacek, M. Barigou, Interpreting the interfacial and colloidal stability of bulk nanobubbles, Soft Matter. 14 (2018) 9643–9656, doi:10.1039/ C8SM01949E
- [51] C.A. Sjogreen, D.A. Landínez Téllez, J.E. Rosas Pérez, P.C. Plazas Hurtado, J. Roa-Rojas, Experimental study of nanobubbles in salt solutions, Rev. La Acad. Colomb. Ciencias Exactas, Físicas y Nat. (2018), doi:10.18257/raccefyn.543.
- [52] S.O. Yurchenko, A.V. Shkirin, B.W. Ninham, A.A. Sychev, V.A. Babenko, N.V. Penkov, N.P. Kryuchkov, N.F. Bunkin, Ion-specific and thermal effects in the stabilization of the gas nanobubble phase in bulk aqueous electrolyte solutions, Langmuir (2016), doi:10.1021/acs.langmuir.6b01644.
- [53] W. Jia, S. Ren, B. Hu, Effect of water chemistry on zeta potential of air bubbles, Int. J. Electrochem. Sci. 8 (2013) 5828–5837.
- [54] P. Leroy, D. Jougnot, A. Revil, A. Lassin, M. Azaroual, A double layer model of the gas bubble/water interface, J. Colloid Interface Sci. 388 (2012) 243–256, doi:10.1016/j.jcis.2012.07.029.
- [55] N.F. Bunkin, A.V. Shkirin, P.S. Ignatiev, L.L. Chaikov, I.S. Burkhanov, A.V. Starosvetskij, Nanobubble clusters of dissolved gas in aqueous solutions of electrolyte. I. Experimental proof, J. Chem. Phys. (2012), doi:10.1063/1.4739528.
- [56] A.S. Najafi, J. Drelich, A. Yeung, Z. Xu, J. Masliyah, A novel method of measuring electrophoretic mobility of gas bubbles, J. Colloid Interface Sci. 308 (2007) 344–350, doi:10.1016/j.jcis.2007.01.014.
- [57] M.Y. Han, M.K. Kim, M.S. Shin, Generation of a positively charged bubble and its possible mechanism of formation, J. Water Supply Res. Technol. - AQUA (2006), doi:10.2166/aqua.2006.055.
- [58] M.Y. Han, M.K. Kim, H.J. Ahn, Effects of surface charge, micro-bubble size and particle size on removal efficiency of electro-flotation, Water Sci. Technol. (2006), doi:10.2166/wst.2006.216.
- [59] S.-H. Cho, J.-Y. Kim, J.-H. Chun, J.-D. Kim, Ultrasonic formation of nanobubbles and their zeta-potentials in aqueous electrolyte and surfactant solutions, Colloids Surfaces A Physicochem. Eng. Asp. 269 (2005) 28–34, doi:10.1016/ j.colsurfa.2005.06.063.
- [60] M.Y. Han, H.J. Ahn, M.S. Shin, S.R. Kim, The effect of divalent metal ions on the zeta potential of bubbles, Water Sci. Technol. (2004), doi:10.2166/ wst.2004.0486.
- [61] K.A. Karraker, C.J. Radke, Disjoining pressures, zeta potentials and surface tensions of aqueous non-ionic surfactant/electrolyte solutions: theory and comparison to experiment, Adv. Colloid Interface Sci. (2002), doi:10.1016/ S0001-8686(01)00083-5.
- [62] C. Yang, T. Dabros, D. Li, J. Czarnecki, J.H. Masliyah, Measurement of the zeta potential of gas bubbles in aqueous solutions by microelectrophoresis method, J. Colloid Interface Sci. (2001), doi:10.1006/jcis.2001.7842.